NASA TECHNICAL NOTE

NASA TN D-6263

NASA TN D-6263



# LIFT AND DRAG CHARACTERISTICS OF THE HL-10 LIFTING BODY DURING SUBSONIC GLIDING FLIGHT

*by Jon S. Pyle*

*Flight Research Center*
*Edwards, Calif. 93523*

NATIONAL AERONAUTICS AND SPACE ADMINISTRATION • WASHINGTON, D. C. • MARCH 1971

| | | |
|---|---|---|
| 1. Report No. NASA TN D-6263 | 2. Government Accession No. | 3. Recipient's Catalog No. |
| 4. Title and Subtitle LIFT AND DRAG CHARACTERISTICS OF THE HL-10 LIFTING BODY DURING SUBSONIC GLIDING FLIGHT | | 5. Report Date March 1971 |
| | | 6. Performing Organization Code |
| 7. Author(s) Jon S. Pyle | | 8. Performing Organization Report No. H-608 |
| 9. Performing Organization Name and Address NASA Flight Research Center P. O. Box 273 Edwards, California 93523 | | 10. Work Unit No. 727-00-00-01-24 |
| | | 11. Contract or Grant No. |
| 12. Sponsoring Agency Name and Address National Aeronautics and Space Administration Washington, D. C. 20546 | | 13. Type of Report and Period Covered Technical Note |
| | | 14. Sponsoring Agency Code |
| 15. Supplementary Notes | | |

16. Abstract

Subsonic lift and drag data obtained during the HL-10 lifting body glide flight program are presented for four configurations for angles of attack from 5° to 26° and Mach numbers from 0.35 to 0.62. These flight data, where applicable, are compared with results from small-scale wind-tunnel tests of an HL-10 model, full-scale wind-tunnel results obtained with the flight vehicle, and flight results for the M2-F2 lifting body.

The lift and drag characteristics obtained from the HL-10 flight results showed that a severe flow problem existed on the upper surface of the vehicle during the first flight test. This problem was corrected by modifying the leading edges of the tip fins. The vehicle attained lift-drag ratios as high as 4.0 during the landing flare (performed with the landing gear up), which is approximately 14 percent higher than demonstrated by the M2-F2 vehicle in similar maneuvers.

| | |
|---|---|
| 17. Key Words (Suggested by Author(s)) Lifting body - Lift-drag ratio - HL-10 vehicle - Flow separation | 18. Distribution Statement Unclassified - Unlimited |

| 19. Security Classif. (of this report) | 20. Security Classif. (of this page) | 21. No. of Pages | 22. Price* |
|---|---|---|---|
| Unclassified | Unclassified | 25 | $3.00 |

*For sale by the National Technical Information Service, Springfield, Virginia 22151

# LIFT AND DRAG CHARACTERISTICS OF THE HL-10 LIFTING BODY DURING SUBSONIC GLIDING FLIGHT

Jon S. Pyle
Flight Research Center

## INTRODUCTION

The concept of manned entry vehicles capable of performing horizontal landings has been the subject of numerous theoretical and experimental studies. Among the many entry configurations studied, extensive wind-tunnel tests were performed to develop an entry shape designated the HL-10 (refs. 1 to 5). In conjunction with these tests, a full-scale HL-10 lifting body vehicle was constructed for use in flight tests through the subsonic, transonic, and supersonic Mach number regions below 2.0. These flight tests are being performed to define the handling characteristics and the landing capability of the vehicle and to confirm the theoretical and wind-tunnel predictions of its stability, control, and performance characteristics.

This paper defines the lift and drag characteristics of the HL-10 vehicle in four configurations over a Mach number range of 0.35 to 0.62 and at angles of attack from 5° to 26°. The flight results, where applicable, are compared with full-scale and small-scale wind-tunnel results and the flight results obtained on an earlier manned lifting body entry vehicle, the M2-F2 (ref. 6).

## SYMBOLS

Physical quantities in this report are given in the International System of Units (SI) and parenthetically in U. S. Customary Units. The measurements were taken in U. S. Customary Units. Details concerning the use of SI, together with physical constants and conversion factors, are given in reference 7.

$\frac{A_c}{S}$ nondimensional cross-sectional area, perpendicular to the vehicle longitudinal axis

$a_l$ longitudinal acceleration, ratio of net aerodynamic force along the vehicle longitudinal axis to vehicle weight, g units

$a_n$ normal acceleration, ratio of net aerodynamic force normal to the vehicle longitudinal axis to vehicle weight, g units

| | |
|---|---|
| $b$ | vehicle span, meters (feet) |
| $C_D$ | drag coefficient, $\frac{D}{qS}$ |
| $\frac{dC_D}{dC_L^2}$ | drag-due-to-lift factor |
| $C_L$ | lift coefficient, $\frac{L}{qS}$ |
| $C_{L_\alpha}$ | lift-curve slope per degree |
| $C_{L_{\delta_e}}$ | variation of lift coefficient with elevator deflection, $\frac{\partial C_L}{\partial \delta_e}$, per degree |
| $C_N$ | normal-force coefficient, $\frac{Wa_n}{qS}$ |
| $C_X$ | axial-force coefficient, $\frac{Wa_l}{qS}$ |
| $D$ | drag force along flight path, newtons (pounds) |
| $g$ | gravitational acceleration, 9.8 meters/second$^2$ (32.2 feet/second$^2$) |
| $L$ | lift force normal to flight path, newtons (pounds) |
| $\frac{L}{D}$ | lift-drag ratio |
| $M$ | free-stream Mach number |
| $M'$ | indicated Mach number |
| $\Delta M$ | Mach-number error, $M - M'$ |
| $N_{Re}$ | Reynolds number, based on vehicle length |

$p$ corrected static pressure, newtons/meter$^2$ (pounds/foot$^2$)

$p'$ indicated static pressure from nose boom, newtons/meter$^2$ (pounds/foot$^2$)

$\Delta p$ position error in static pressure, $p' - 1$, newtons/meter$^2$ (pounds/foot$^2$)

$q$ dynamic pressure, newtons/meter$^2$ (pounds/foot$^2$)

$S$ reference area, body planform, meters$^2$ (feet$^2$)

$W$ vehicle weight, kilograms (pounds)

$\frac{x}{l}$ ratio of distance from nose of vehicle to an arbitrary point along longitudinal axis to total vehicle length

$\alpha$ true angle of attack, $\alpha_m + \Delta\alpha_\beta + \Delta\alpha_q + \Delta\alpha_\epsilon + \Delta\alpha_c$, degrees

$\alpha_m$ measured angle of attack, degrees

$\Delta\alpha_c$ angle of attack correction at 0° angle of attack, due to angular difference between nose-boom incidence and the vehicle's longitudinal axis, degrees

$\Delta\alpha_q$ angle-of-attack correction for effect of pitching rates on angle-of-attack vane, degrees

$\Delta\alpha_\beta$ angle-of-attack correction for nose-boom bending due to normal force, degrees

$\Delta\alpha_\epsilon$ angle-of-attack correction for effect of upwash factor on angle-of-attack vane, $\left(\frac{\Delta\alpha_\epsilon}{\alpha_m}\right)\alpha_m$, degrees

$\delta_e$ elevon deflection, degrees

$\delta_{sb}$ speed-brake deflection, degrees

$\sigma$ root-mean-square error

Subscripts:

| | |
|---|---|
| max | maximum |
| mean | average between right and left elevon deflections |
| min | minimum |

## VEHICLE DESCRIPTION

The HL-10 is a wingless, lifting configuration with a delta planform and negative camber. Heating was not a problem at the low Mach numbers of these flight tests, therefore aluminum was the primary material used to construct the vehicle's semi-monocoque structure. The pertinent physical characteristics of the vehicle are presented in table 1, and photographs are shown in figures 1(a) and (b).

TABLE 1. PHYSICAL CHARACTERISTICS OF THE HL-10 VEHICLE

| | |
|---|---|
| Body — | |
| Reference planform area, meters$^2$ (feet$^2$) | 14.9 (160) |
| Length, meters (feet) | 6.45 (21.17) |
| Span, meters (feet) | 4.15 (13.6) |
| Aspect ratio (basic vehicle), $\frac{b^2}{S}$ | 1.156 |
| Weight, including pilot, kilograms (pounds) | 2722 (6000) |
| Center of gravity, percentage of reference length | 51.8 |
| Base area: | |
| Configuration A and B, meters$^2$ (feet$^2$) | 1.38 (14.83) |
| Configuration C, meters$^2$ (feet$^2$) | 1.57 (16.98) |
| Configuration D, meters$^2$ (feet$^2$) | 2.71 (29.13) |
| Elevons (two) — | |
| Area, each, meters$^2$ (feet$^2$) | 1.00 (10.72) |
| Span, each, parallel to hinge line, meters (feet) | 1.09 (3.58) |
| Chord, perpendicular to hinge line: | |
| Root, meters (feet) | 0.59 (1.93) |
| Tip, meters (feet) | 1.24 (4.06) |
| Elevon flaps (two) — | |
| Area, each, meters$^2$ (feet$^2$) | 0.70 (7.50) |
| Span, each, parallel to hinge line, meters (feet) | 1.09 (3.58) |
| Chord, perpendicular to hinge line: | |
| Root, meters (feet) | 0.48 (1.58) |
| Tip, meters (feet) | 0.80 (2.63) |
| Vertical stabilizer (one) — | |
| Area, meters$^2$ (feet$^2$) | 1.47 (15.8) |
| Height, trailing edge, meters (feet) | 1.53 (5.02) |
| Chord: | |
| Root, meters (feet) | 1.32 (4.32) |
| Tip, meters (feet) | 0.60 (1.97) |
| Leading-edge sweep, degrees | 25 |
| Rudders (two) — | |
| Area, each, meters$^2$ (feet$^2$) | 0.41 (4.45) |
| Height, each, meters (feet) | 1.26 (4.12) |
| Chord, meters (feet) | 0.33 (1.08) |
| Outboard tip-fin flaps (two) — | |
| Area, each, meters$^2$ (feet$^2$) | 0.35 (3.77) |
| Height, hinge line, meters (feet) | 1.37 (4.50) |
| Chord, perpendicular to hinge line, meters (feet) | 0.26 (0.84) |
| Inboard tip-fin flaps (two) — | |
| Area, each, meters$^2$ (feet$^2$) | 0.23 (2.48) |
| Height, hinge line, meters (feet) | 1.01 (3.31) |
| Chord, perpendicular to hinge line, meters (feet) | 0.23 (0.75) |

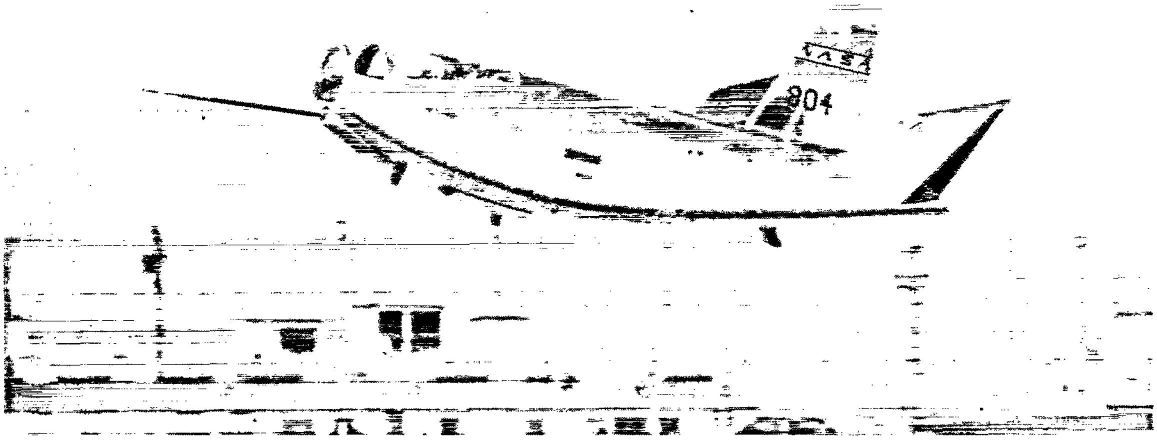


*(a) Gear up.*

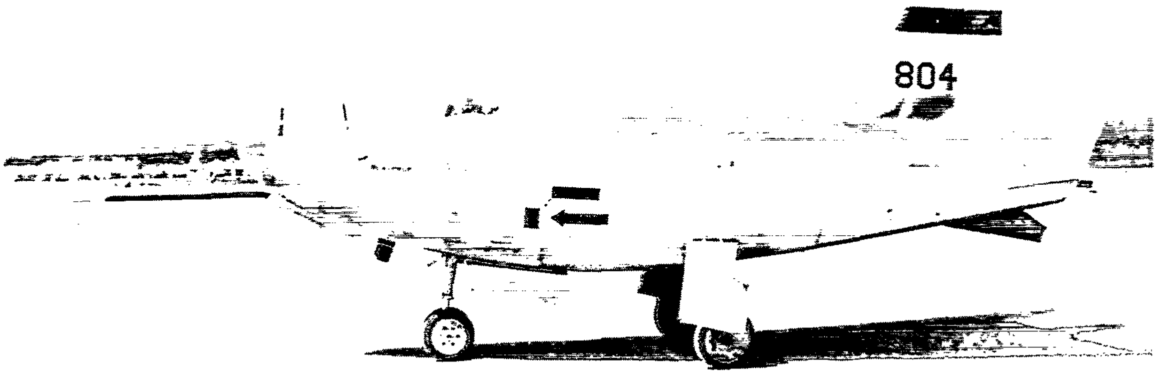


*(b) Gear down.*

*Figure 1. HL-10 vehicle.*

Figure 2 is a three-view drawing of the vehicle with dimensions and control surfaces specified. The elevons, which are the primary control surfaces, provide both pitch and roll control; the rudders, located on the center vertical stabilizer, provide directional control and function as speed brakes with symmetrical outward deflection. In addition to the primary control surfaces, secondary surfaces are located on the tip fins and the upper surfaces of the elevons. These secondary surfaces are used to change the vehicle configuration during flight and are adjustable by the pilot.

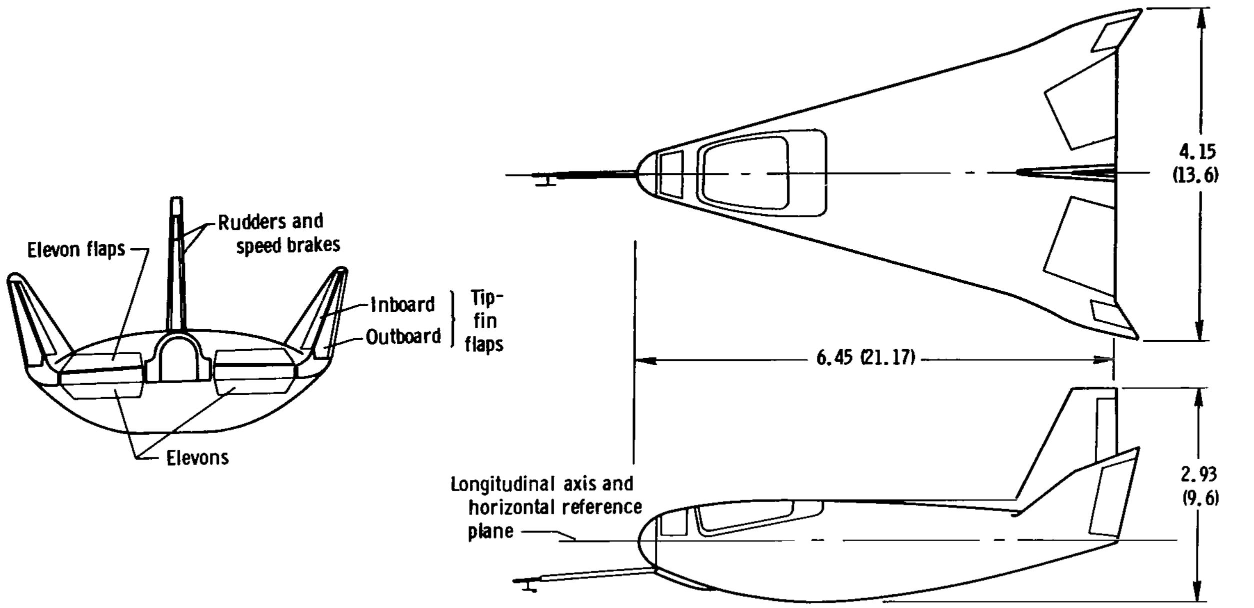


*Figure 2. Three-view drawing of HL-10 vehicle. (Dimensions in meters (feet)).*

Configurations A and B (fig. 3) were designed for maximum vehicle stability in the subsonic Mach number region (M < 0.6). Configuration A was used during the full-scale wind-tunnel tests (ref. 8) and the initial flight test. However, during the initial

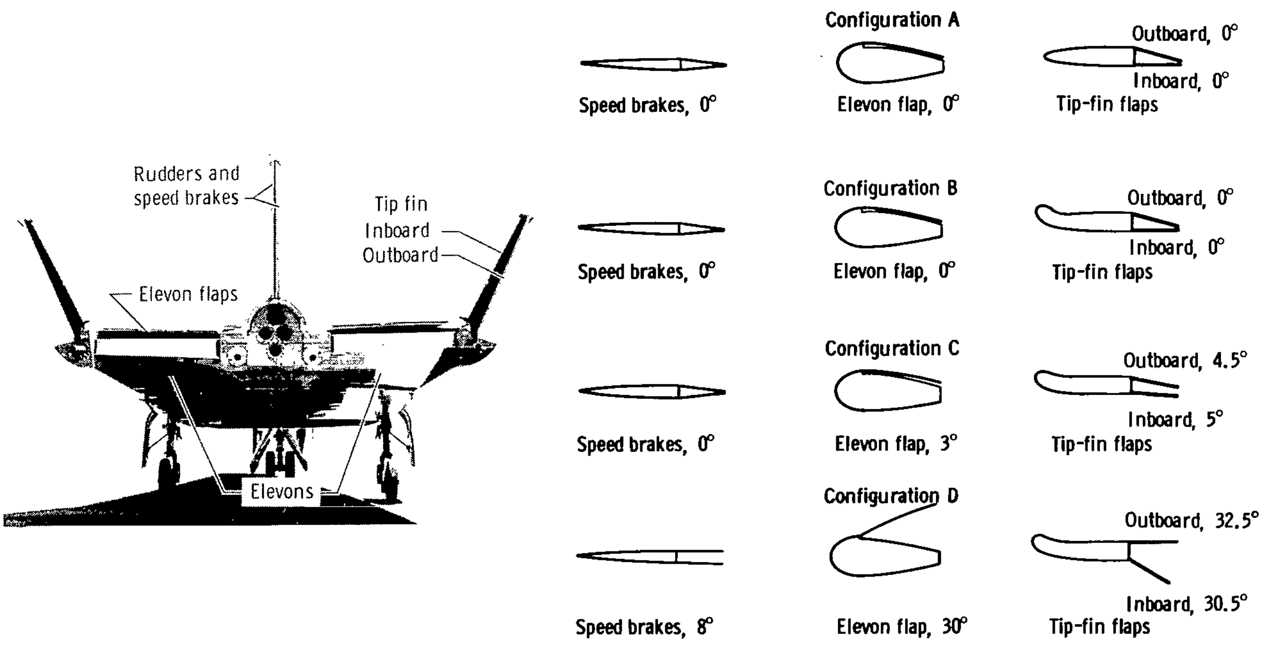


*Figure 3. HL-10 secondary control surfaces in alternate configurations.*

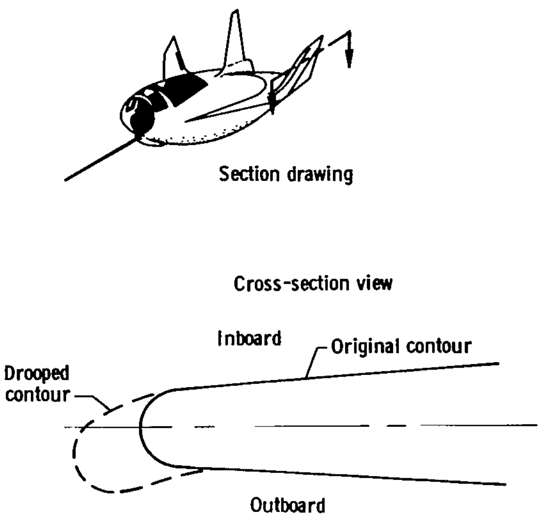


*Figure 4. HL-10 tip-fin modification.*

flight test, a severe flow disturbance was encountered on the vehicle's upper surface. To alleviate the control and performance problems caused by this flow disturbance, the leading edges of the tip fins were drooped (fig. 4) to divert additional flow over the vehicle's upper surface. This modification is the only physical difference between configurations A and B (fig. 3).

After preliminary tests with configuration B, an interim configuration (C) was used. For this configuration small changes were made in the deflections of the secondary control surfaces (fig. 3) which increased the vehicle's usable angle-of-attack range but did not significantly alter its longitudinal-stability characteristics. Subsequent flight tests in the subsonic Mach number region ($M < 0.6$) were made with configuration C.

To alleviate stability problems encountered at the higher Mach numbers, the secondary control surfaces were deflected significantly (fig. 3, configuration D). Deflecting these surfaces increased the base area of the vehicle and thus resulted in greater longitudinal stability at Mach numbers above 0.6 (transonic Mach number region).

Figure 5 shows the variation of the nondimensional cross-sectional area of the vehicle with percent of body length. The wing loading was approximately 183 kilograms/meter$^2$ (37.5 pounds/foot$^2$), based on the reference planform area of 14.9 meters$^2$ (160 feet$^2$). The center of gravity for these tests was approximately 51.8 percent of the reference length.

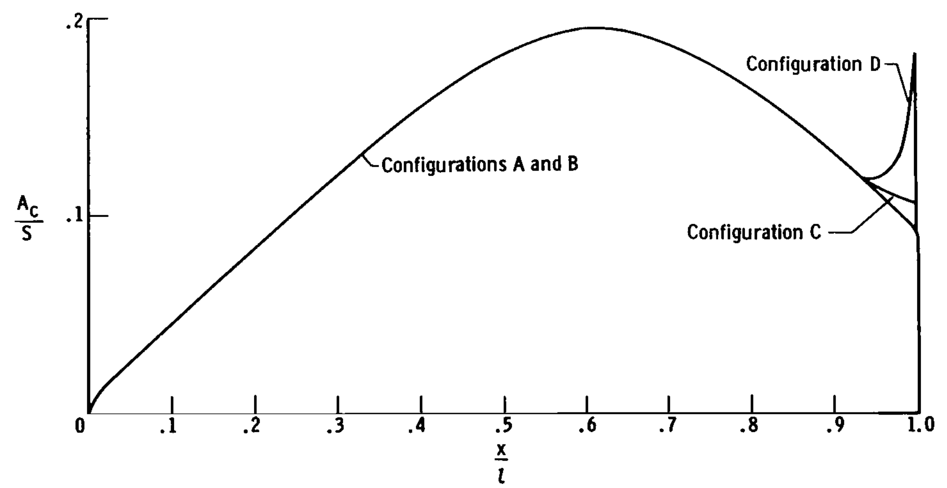


*Figure 5. HL-10 cross-sectional-area distribution.*

## TEST CONDITIONS

### Flight

The flight lift and drag results presented were obtained during glide flights of the HL-10 vehicle with the landing gear up, following launch from a B-52 airplane. The data were obtained at altitudes below 13,700 meters (45,000 feet) and at Mach numbers between 0.35 and 0.62. The vehicle angle of attack was varied from 5° to 26°, and the Reynolds numbers ranged from $25 \times 10^6$ to $62 \times 10^6$, based on the vehicle length of 6.45 meters (21.17 feet).

### Wind Tunnel

Full scale.– Prior to the flight tests of the HL-10 vehicle, wind-tunnel tests were conducted with the flight vehicle in the NASA Ames Research Center's 40- by 80-foot wind tunnel (ref. 8). The data were obtained with the tip fins in the original contour (fig. 4), thus they are compared with the flight data obtained from the vehicle before the tip-fin leading edges were modified.

Small scale.– A 0.063-scale model of the HL-10 vehicle was tested in the NASA Langley Research Center's high-speed 7- by 10-foot wind tunnel (ref. 9). Tests were made with the model in configuration A (unmodified tip-fin contours), B, and D (modified tip-fin contours). The wind-tunnel tests were conducted over a Mach number range of 0.35 to 0.9. The test Reynolds number varied from $2.7 \times 10^6$ to $4.0 \times 10^6$, based on the model length of 0.403 meter (1.322 feet).

Base pressure measurements were obtained during the small-scale wind-tunnel tests. The effects of sting interference on the model base pressures and on the flow over the surfaces ahead of the base were assumed to be negligible, although adequate wind-tunnel and flight base-pressure measurements have not been compared to substantiate this assumption.

The wind-tunnel drag results were adjusted for approximately an order-of-magnitude difference in Reynolds number between the flight and model tests. This adjustment was derived from the Kármán-Schoenherr flat-plate relationship modified for compressibility effects by the method of Sommer and Short (ref. 10). The resulting increment of drag was applied to the model values of $C_D$ and $\frac{L}{D}$ as a constant reduction of drag coefficient of 0.0035 and are shown in the following discussion as an adjustment to the small-scale wind-tunnel results. Three-dimensional and lift effects on this increment were assumed to be negligible; similarly, the viscous effects attributable to scale differences on parameters other than drag were not considered.

## METHOD OF MEASUREMENT

Measurements of normal and longitudinal accelerations were used to determine lift and drag. The equations used in this method are developed in reference 11. The following relationships apply to the data presented:

$$C_L = C_N \cos \alpha - C_X \sin \alpha$$

$$C_D = C_X \cos \alpha + C_N \sin \alpha$$

## INSTRUMENTATION

### Description

The accelerations of the HL-10 vehicle were measured by sensitive accelerometers mounted as close as possible to the vehicle's center of gravity. Corrections to the accelerometer measurements because of the displacement of the instruments from the center of gravity were found to be negligible. A standard NACA nose boom was used to measure static and impact pressure (ref. 12) and angles of attack and sideslip. Angle of attack was measured by a floating vane attached to the nose boom and positioned 1.5 meters (4.8 feet) forward of the vehicle's nose. The static- and impact-pressure orifices were 1.73 meters (5.68 feet) and 1.94 meters (6.35 feet), respectively, forward of the nose. All data obtained from the onboard instrumentation were telemetered to ground recording stations by using a pulse-code-modulation system.

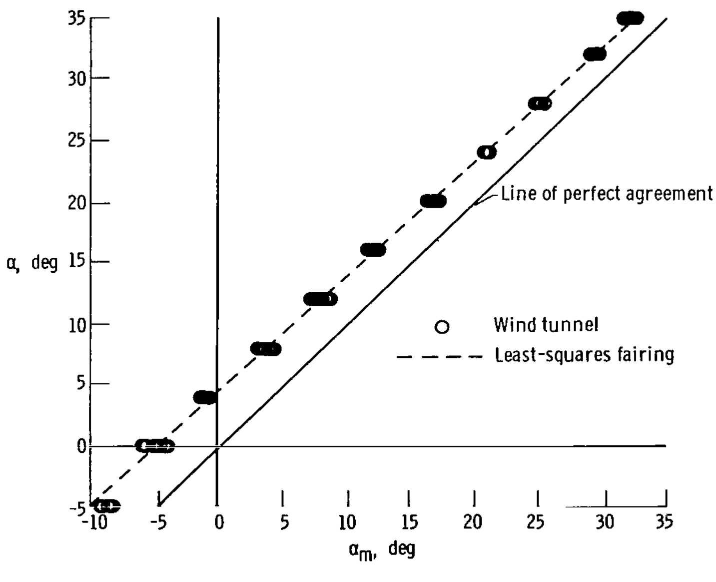


*Figure 6. Full-scale wind-tunnel angle-of-attack calibration for the HL-10 vehicle. M = 0.2.*

### Special Calibrations

Angle of attack.– Figure 6 presents the results of an angle-of-attack calibration of the floating vane attached to the nose boom performed at a Mach number of 0.2 in the full-scale wind tunnel (ref. 8). From this calibration, an angle-of-attack correction, $\Delta\alpha_c$, was obtained at 0° angle of attack which was primarily due to the angular difference between the nose-boom incidence and the vehicle's longitudinal axis. The upwash effect of the nose boom and fuselage on the angle-of-attack vane, $\Delta\alpha_\epsilon$, was assumed to be approximated by the difference between the slope of the calibrated angle-of-attack curve and the line of perfect agreement. The total wind-tunnel upwash value for a Mach number of 0.2 is represented by the solid circle in figure 7.

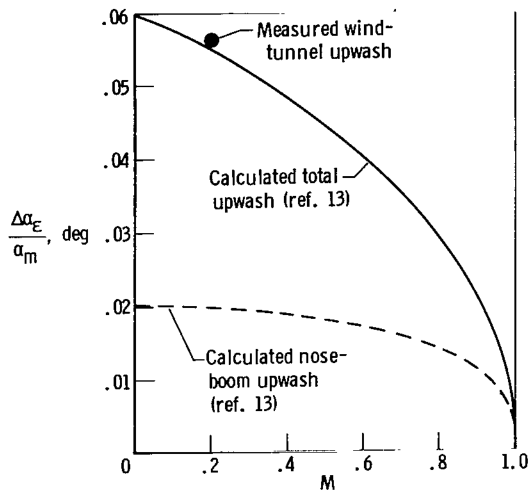


*Figure 7. Upwash factor for the HL-10 angle-of-attack vane.*

The estimated correction for the total upwash effect on the angle-of-attack vane through the subsonic Mach number range was calculated as a function of $\alpha_m$ by using the method of reference 13. The calculated nose-boom upwash is shown as a dashed line in figure 7. The body upwash effect was more complicated to calculate because of the asymmetric shape of the vehicle in the longitudinal plane. However, a calculation was made by using radii obtained from the HL-10 cross-sectional-area distribution (fig. 5) for an equivalent body of revolution. The calculated body upwash added to the nose-boom upwash is shown in figure 7 by the solid line; it agrees closely with the estimated total upwash obtained from the wind-tunnel results at Mach 0.2. The correction $\Delta\alpha_\epsilon$ due to the calculated total upwash factor can thus be obtained from figure 7 and measured angle of attack, $\alpha_m$.

The angle-of-attack vane was calibrated for the effect of boom bending, $\Delta\alpha_\beta$, due to normal accelerations. A correction for pitching rate, $\Delta\alpha_q$, for the angle-of-attack vane located 5.35 meters (17.55 feet) forward of the vehicle's center of gravity was also determined. The corrections applied to the flight-measured angle of attack to obtain the true angle of attack were as follows:

$$\alpha = \alpha_m + \Delta\alpha_\beta + \Delta\alpha_q + \Delta\alpha_\epsilon + \Delta\alpha_c$$

Air-data measurements. – The pressure data sensors were calibrated for static-pressure and Mach-number position error by comparing the flight-measured static pressure with an ambient pressure measured with a radiosonde balloon. The relationship of ambient pressure to altitude was obtained by using the hydrostatic equation. The altitude of the vehicle during flight was measured by radar, thus permitting comparison of the ambient pressures measured by the onboard instrumentation with the radiosonde results. The calibration of position error as a function of indicated Mach number is shown in figures 8(a) and 8(b).

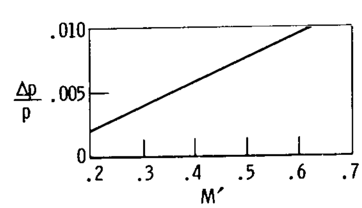


*(a) Static-pressure error.*

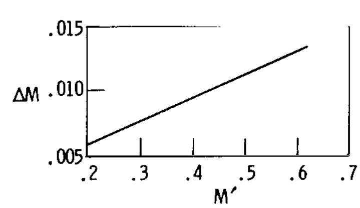


*(b) Mach-number error.*

*Figure 8. Position error of the airspeed system used on the HL-10 vehicle.*

## ERRORS AND RELIABILITY

The standard deviations of the quantities used to calculate lift and drag, including instrument, transmission, and data-reduction-system errors, are as follows:

| | |
|---|---|
| W, kilograms (pounds) . . . . . . . . . . . . . . | ±2.3 (±5) |
| $a_n$, g . . . . . . . . . . . . . . . . . . . . . . . . | ±0.014 |
| $a_l$, g . . . . . . . . . . . . . . . . . . . . . . . . | ±0.003 |
| q, newtons/meter$^2$ (pounds/foot$^2$) . . . . . . . | ±96 (±2) |
| $\alpha$, degrees . . . . . . . . . . . . . . . . . . . . | ±0.5 |
| M . . . . . . . . . . . . . . . . . . . . . . . . . . . | ±0.01 |

It is of interest to examine whether the errors of these individual measurements are random or biased. Errors such as those inherent in the measurement of weight are biased for each flight; however, these biased errors should become random when data from several flights are used. The individual measurement errors of the accelerometers, pressure sensors, and angle-of-attack sensors are random. The biased errors which may occur in these quantities are reduced by careful calibrations, correction to zero shifts, and proper location of the instruments within the vehicle. Because most of the errors are random, fairing the flight data should significantly reduce the net error. The scatter in the flight data increased appreciably during extreme transient pitch motions; therefore, all flight data with pitch rates above ±5 degrees/second were discarded.

The net random error in the measurement of lift and drag is best represented by the root-mean-square summation of the random errors. The effect of each error upon evaluations of the lift coefficient, drag coefficient, and lift-drag ratio are tabulated below. These errors are typical of the types found in flight results for a lift-drag ratio of 3.55 and a dynamic pressure of 12,000 newtons/meter$^2$ (250 pounds/foot$^2$) and would be typical for most subsonic Mach numbers.

| Quantity | $\frac{dC_L}{C_L}$, percent | $\frac{dC_D}{C_D}$, percent | $\frac{d\frac{L}{D}}{\frac{L}{D}}$, percent |
|---|---|---|---|
| W | ±0.8 | ±0.8 | -- |
| $a_n$ | ±1.3 | ±1.4 | Negligible |
| $a_l$ | Negligible | ±1.0 | Negligible |
| q | ±1.4 | ±1.4 | -- |
| $\alpha$ | ±2.5 | ±3.1 | ±3 |
| $\sigma$ | ±3.25 | ±3.9 | ±3 |

## DISCUSSION

### Configuration A

Some lift and drag results for configuration A were obtained during the first flight of the HL-10 vehicle. These data are presented as faired curves in figures 9(a) and 9(b) for three Mach numbers and are compared with the results obtained from the similar small-scale wind-tunnel model (adjusted for scale effects) and the vehicle in the full-scale wind tunnel. The flight and wind-tunnel lift characteristics are in

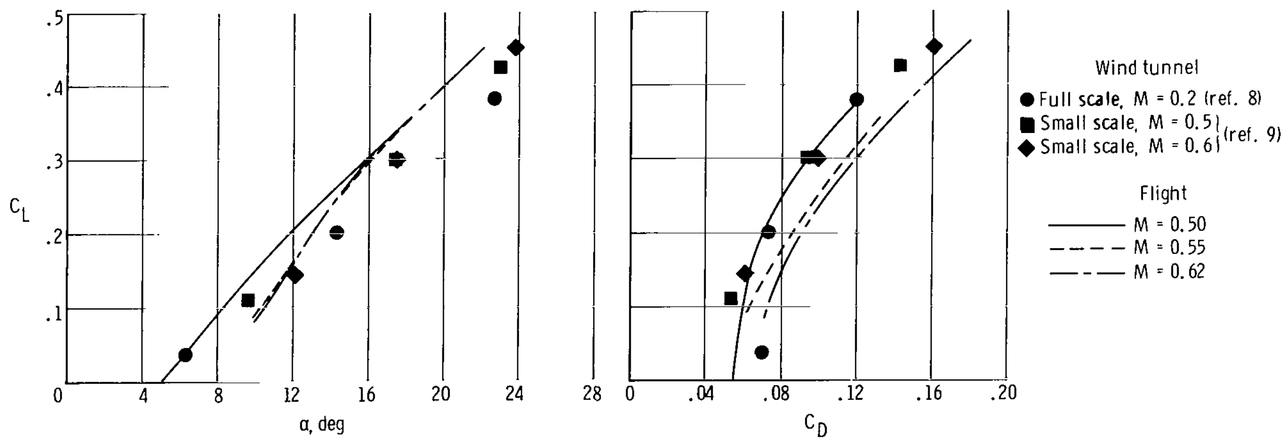


*(a) Lift curves and drag polars.*

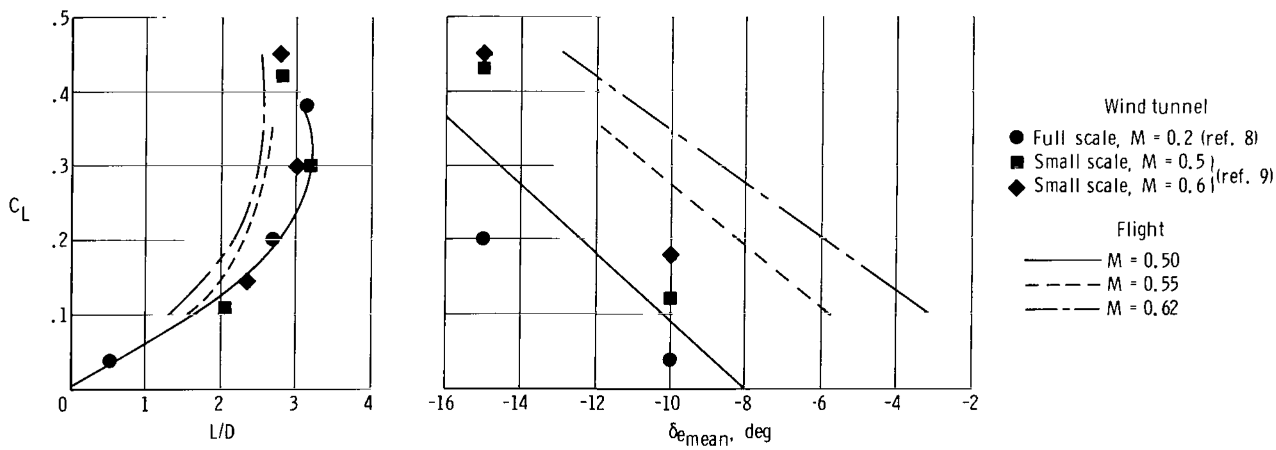


*(b) Lift-drag ratios and elevon deflections.*

*Figure 9. Lift and drag characteristics of the HL-10 vehicle in Configuration A.*

generally poor agreement. The flight drag data at a Mach number of 0.50 agree reasonably well with both wind-tunnel results. The flight results indicate a significant difference in the lift and drag characteristics between Mach numbers of 0.50 and 0.62. This difference is also apparent in figure 10, which compares the flight maximum lift-drag ratios and the corresponding full-scale and small-scale wind-tunnel results. The data are presented in this manner to show the obvious decrease in the flight lift-drag ratio at a Mach number just above 0.5. This abrupt change indicates the onset of flow separation over the upper surface of the vehicle which may have been caused by an adverse pressure gradient over the inside surfaces of the tip fins. However, the small-scale wind-tunnel data show a more gradual decrease in $\left(\frac{L}{D}\right)_{max}$ at the higher Mach numbers and indicate a gradual growth of regions of separated flow at Mach numbers above 0.6. This severe flow separation was alleviated by a major modification of the tip-fin leading edges, as discussed in the following section.

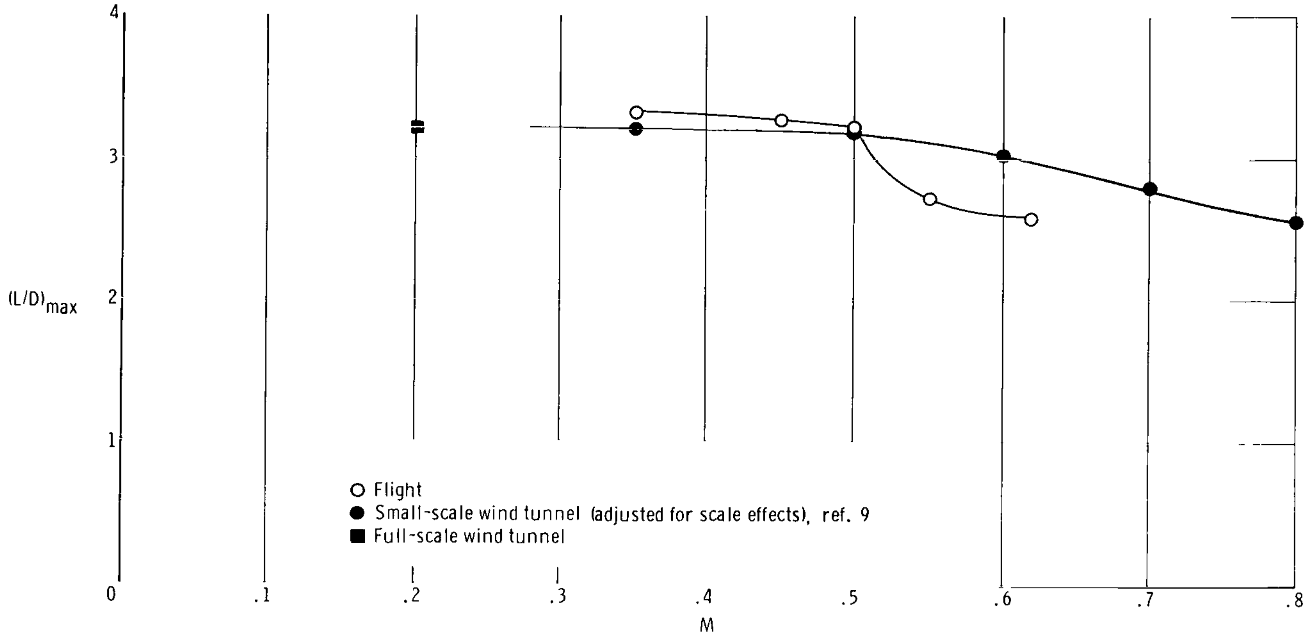


*Figure 10. Mach number effect on the maximum lift-drag ratio of the HL-10 vehicle in configuration A.*

## Configuration B

After the first flight, the vehicle was modified to configuration B by incorporating droop in the leading edges of the outboard tip fins (figs. 3 and 4). Lift and drag data obtained in this configuration at a flight Mach number of 0.6 and a Reynolds number of $30 \times 10^6$, based on the vehicle length, are presented in figures 11(a) and 11(b).

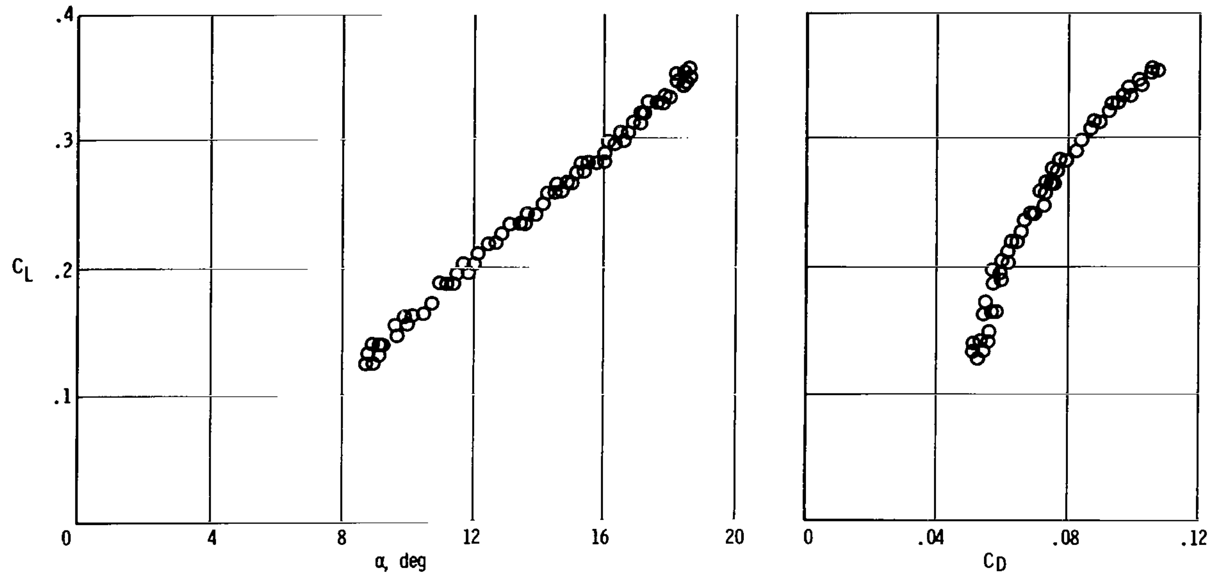


*(a) Lift curve and drag polar.*

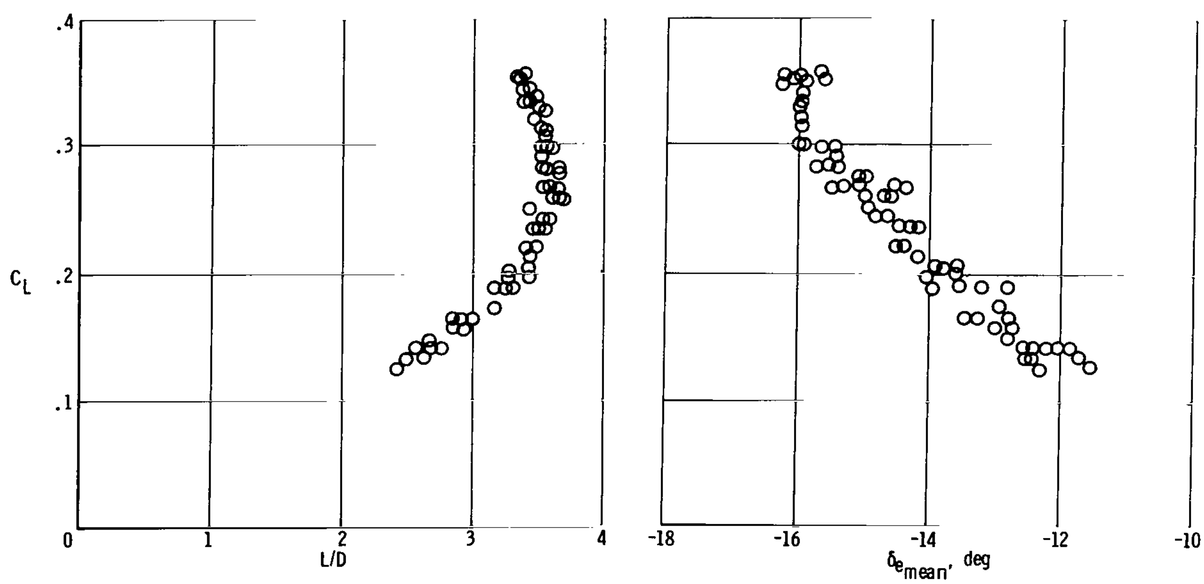


*(b) Lift-drag ratios and elevon deflections.*

*Figure 11. Lift and drag characteristics of the HL-10 vehicle in configuration B. M = 0.6.*

Small-scale-model wind-tunnel results (adjusted for scale effects) obtained with the vehicle in configuration B are presented in figure 12 for comparison with the corresponding flight results obtained by fairing the data of figure 11. The pertinent

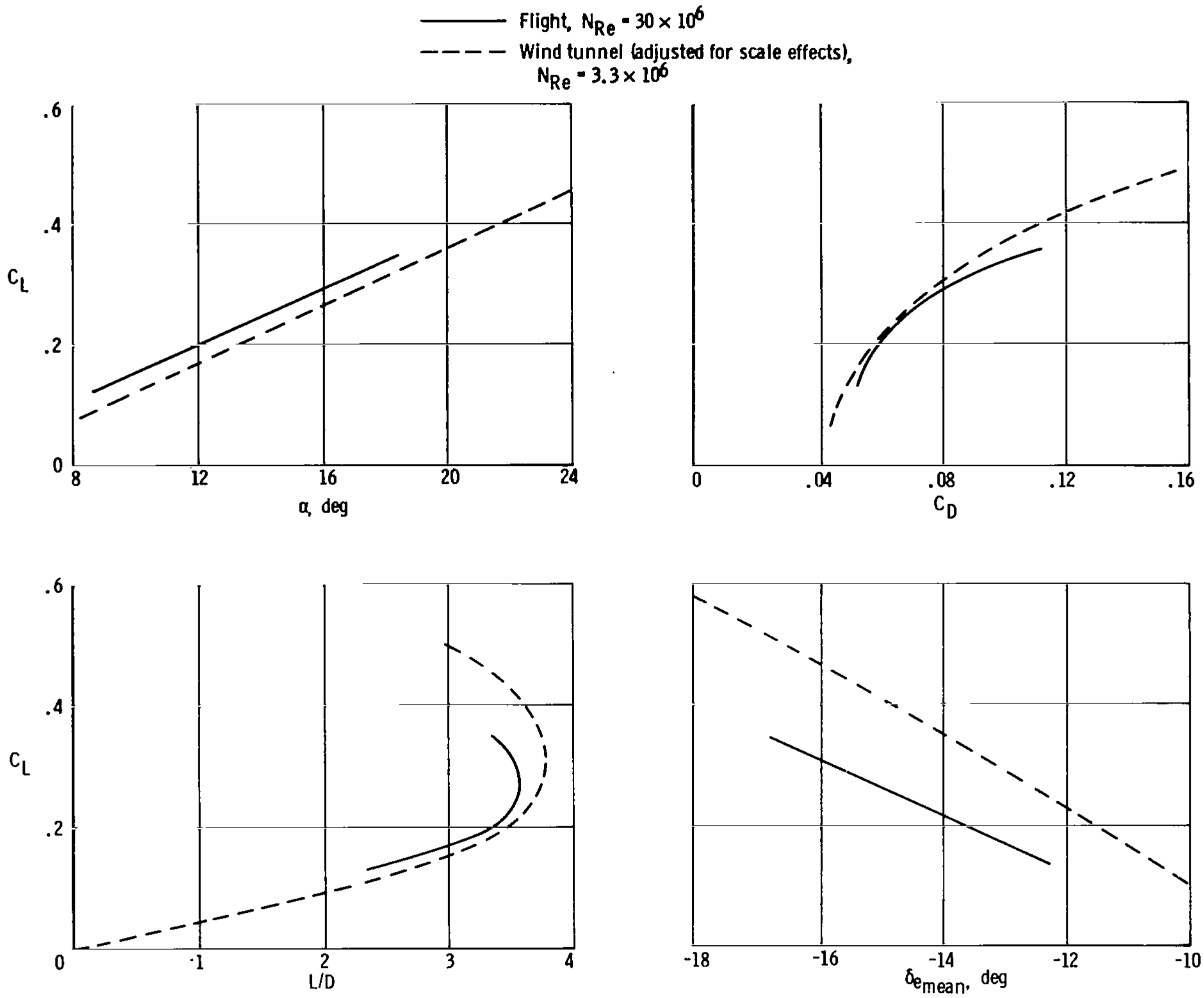


*Figure 12. Comparison of results obtained from tests of a small-scale wind-tunnel model and from flight tests of the HL-10 vehicle in configuration B. M = 0.6.*

lift and drag parameters obtained from the flight and wind-tunnel results are presented in the following table:

| Test | $C_{L_\alpha}$ per deg | $(C_D)_{min}$ | $\frac{dC_D}{dC_L^2}$ | $\left(\frac{L}{D}\right)_{max}$ | $C_{L_{\delta_e}}$ per deg |
|---|---|---|---|---|---|
| Flight | 0.023 | 0.050 | 0.492 | 3.60 | 0.049 |
| Wind tunnel | .024 | .042 | .463 | 3.77 | .061 |

Previous comparisons of results from a blunt-body model and flight vehicle (ref. 14) showed substantial evidence that the model support sting significantly influenced the drag of the model. The support sting increased the base pressure of the model, thus reducing the measured drag. The base pressures (unpublished) of the HL-10 vehicle obtained in flight indicate that the base may cause as much as 30 percent of the zero-lift drag at the subsonic speeds investigated. However, a meaningful comparison of the flight-to-model support sting influence has not been made because adequate data are not yet available.

Detailed examination of the data in figure 12 indicates that to generate any specific lift coefficient the flight vehicle requires greater elevon deflection and less angle of attack than had been predicted by the small-scale wind-tunnel results. This difference in trim altered the configuration of the vehicle, thus contributing to the significant difference in the shape of the drag polar between the model and flight results.

The flight results (M = 0.6) for configuration A are presented in figure 13 for comparison with flight data obtained after the vehicle was modified by drooping the leading edges of the tip fins. The results obtained with configuration A include data which indicated the presence of flow separation over the upper surface of the vehicle (mentioned previously). The drag data for the modified vehicle (configuration B) show a significant reduction in the basic drag and an appreciable gain in the lift-drag ratio when compared with the results for configuration A. This drag reduction indicates that the modification to the leading edges of the tip fins reduced the flow separation over the upper surface of the vehicle.

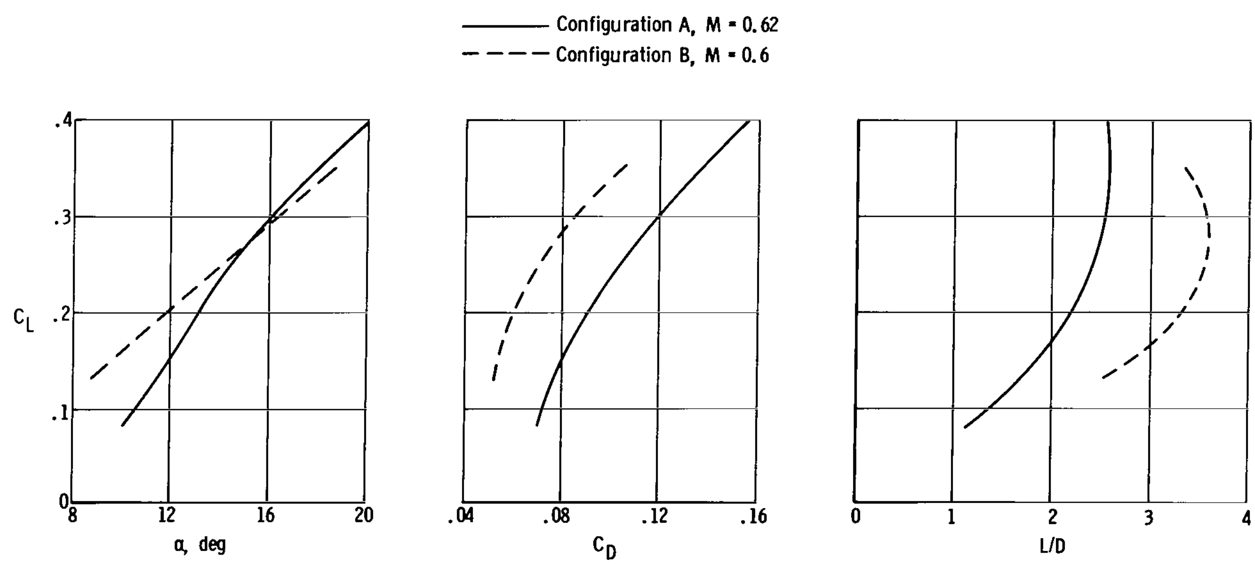


*Figure 13. Comparison of the lift and drag characteristics of the HL-10 vehicle in configurations A and B.*

## Configuration C

In configuration B the vehicle was limited to a maximum angle of attack by the maximum available control deflection provided by the mechanical linkage of the control system. Although this maximum angle of attack was adequate for control of the vehicle under most flight conditions, the limit was believed to be marginal for the landing maneuver. Therefore, the configuration was modified to configuration C (fig. 3), which provided an increased nose-up pitching moment and allowed the vehicle to be flown at a higher angle of attack.

The lift and drag characteristics of the vehicle in configuration C are presented in figure 14 for a Mach number of 0.6 and a Reynolds number of $25 \times 10^6$, based on the vehicle length. The data indicate excellent repeatability of the lift and drag results from several flights. The results for the lift curve and drag polar (fig. 14 (a)) and

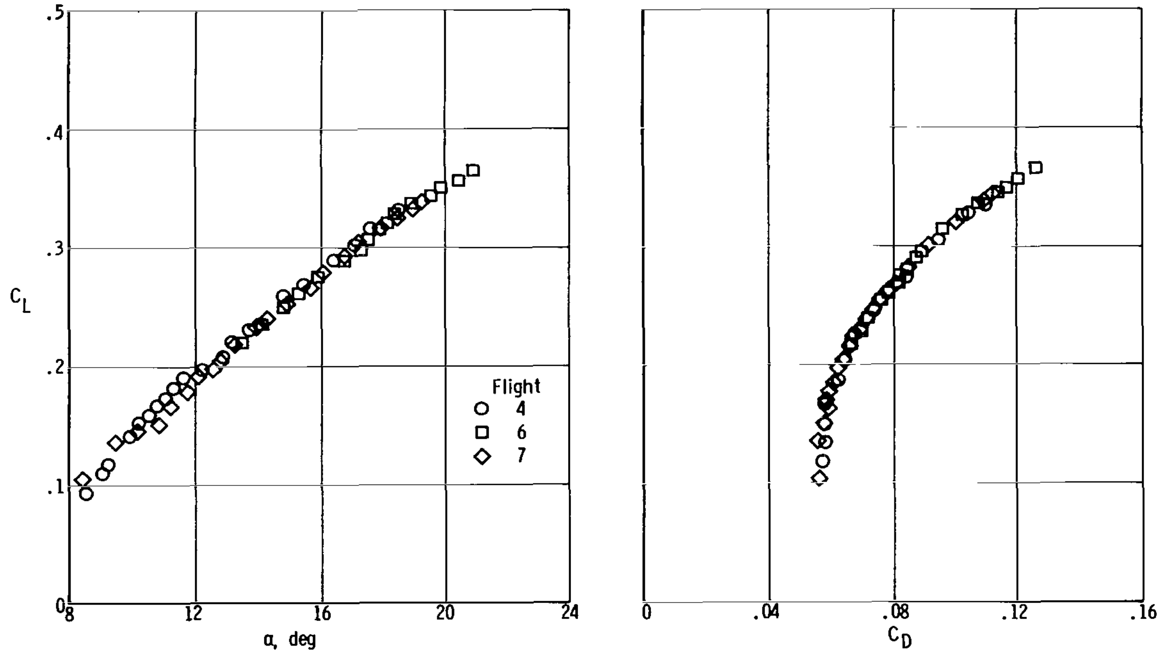


*(a) Lift curve and drag polar.*

*Figure 14. Lift and drag characteristics of the HL-10 vehicle in configuration C obtained from three flights. M = 0.6.*

variation of mean elevon deflection with lift coefficient (fig. 14(b)) represent a sampling of data points from four separate maneuvers during three flights. The approximately 500 data points for the lift-drag ratio (fig. 14(b)) represent the total number of samples taken from these four maneuvers. The points show a maximum scatter of ±3 percent from a faired data curve.

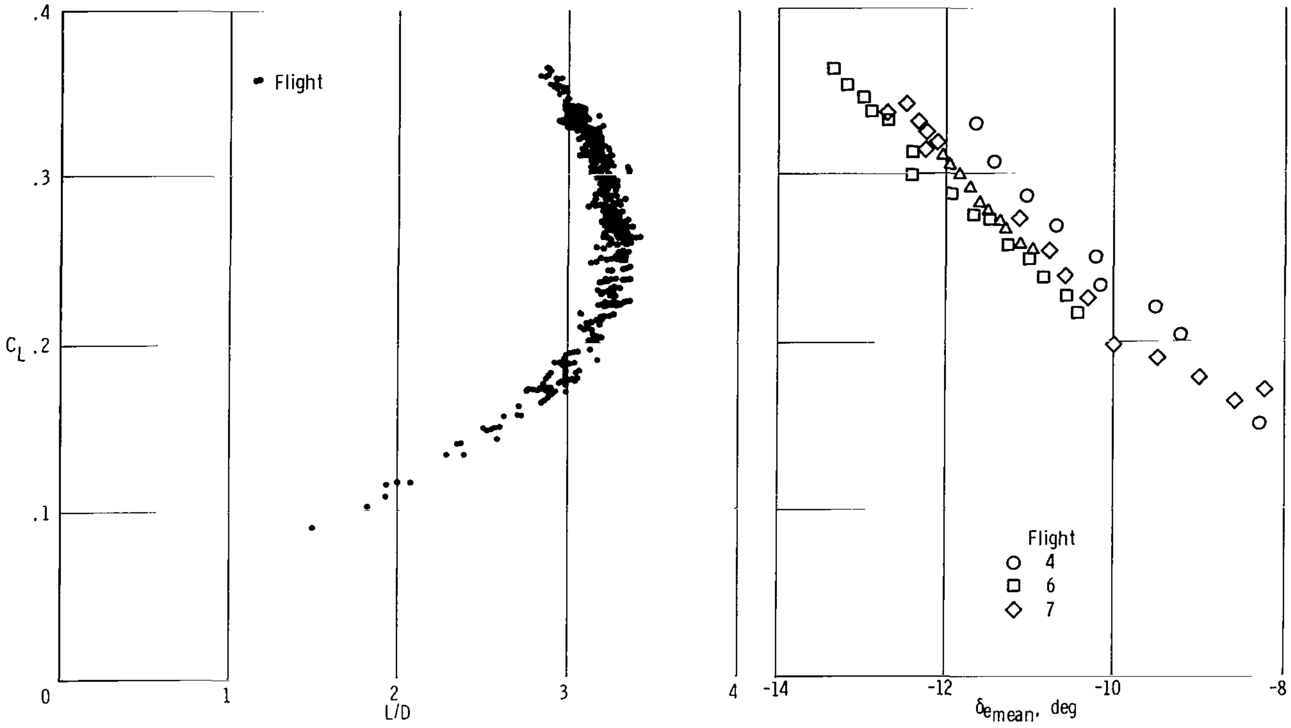


*(b) Lift-drag ratios and elevon deflections.*

*Figure 14. Concluded.*

The principal lift and drag data for configurations B and C obtained from the flight results are compared in the following table:

| Configuration | $C_{L_\alpha}$ per deg | $(C_D)_{min}$ | $\frac{dC_D}{dC_L^{\ 2}}$ | $\left(\frac{L}{D}\right)_{max}$ | $C_{L_{\delta_e}}$ per deg |
|---|---|---|---|---|---|
| B | 0.023 | 0.050 | 0.492 | 3.60 | 0.049 |
| C | .021 | .055 | .571 | 3.33 | .049 |

The data for the two configurations indicate excellent agreement in lift-curve slope. The increase in minimum drag coefficient and decrease in maximum lift-drag ratio for configuration C was expected, because of the increased deflections of the secondary control surfaces. Although the slopes of the $C_{L_{\delta_e}}$ curves are similar, 4° less elevon deflection was necessary to obtain any specific lift coefficient with configuration C. (Compare fig. 11(b) with fig. 14(b).) This decrease in elevon deflection for a particular lift coefficient provided the pilot with the additional longitudinal control, hence angle-of-attack capability, needed for the landing maneuver.

Some faired flight results are presented in figure 15 for configuration C at Reynolds numbers of $25 \times 10^6$, $45 \times 10^6$, and $62 \times 10^6$ and Mach numbers of 0.60, 0.58 to 0.55,

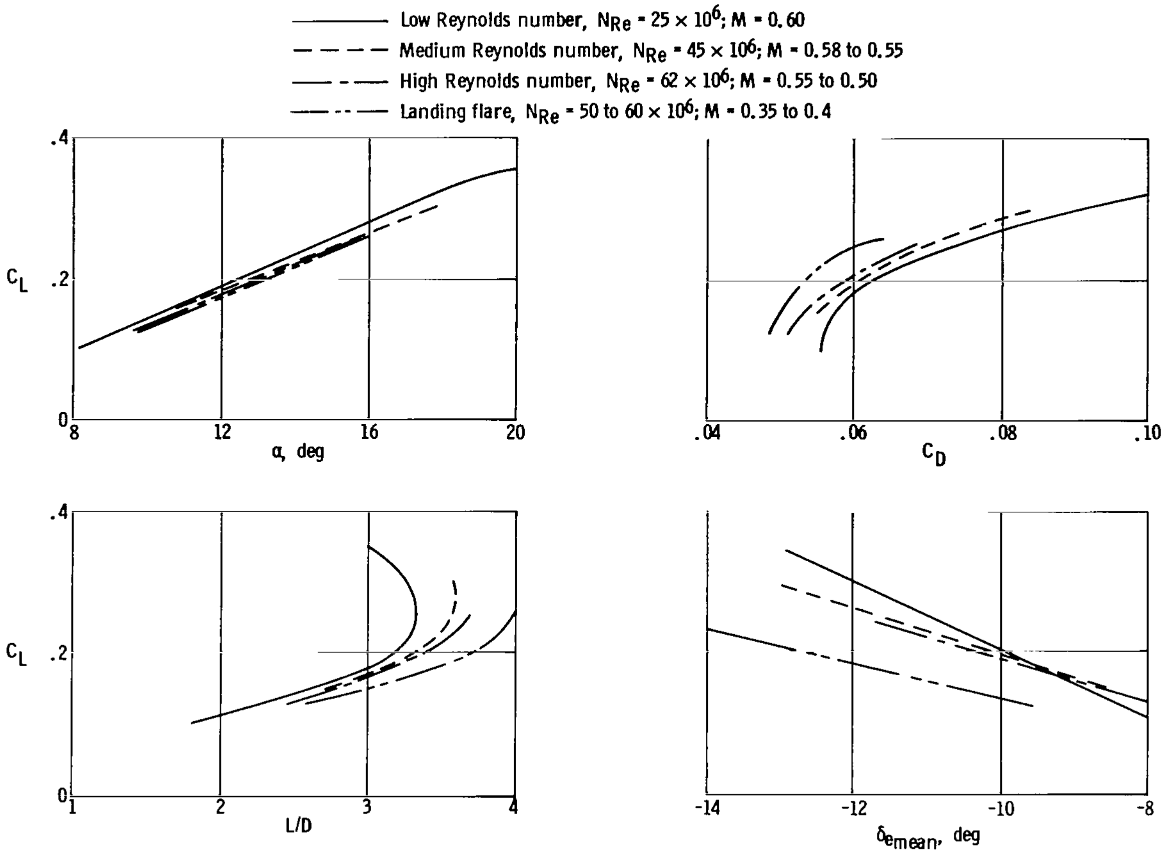


*Figure 15. Effect of Reynolds number and Mach number on the lift and drag characteristics of the HL-10 vehicle in configuration C.*

and 0.55 to 0.50, respectively. The variation in drag coefficient indicates some influence of the Reynolds number variation. The differences in drag (and, hence, maximum lift-drag ratio) could, at first, be attributed to differences in the elevon deflection; however, further examination of the data indicates that, for the lowest Reynolds number, the lowest $\left(\frac{L}{D}\right)_{max}$ (highest $C_D$) was obtained with the least amount of elevator deflection. Thus, an adjustment of the drag for the effect of the differences in elevon deflection would tend to increase the difference in the drag due to Reynolds number. Adequate flight results at a constant Mach number were not available to define the effects of Reynolds number independently from those of Mach number, thus some of the noted decrease in drag may be due to the reduction in Mach number.

Lift and drag characteristics obtained during a typical HL-10 landing flare are also presented in figure 15. These results are not directly comparable to the previously discussed data at a constant Reynolds number because of the lower Mach number and the Reynolds number variation during the landing maneuver. The data are presented to show that the HL-10 vehicle attained lift-drag ratios of 4.0 during the glide-flight program, and, for essentially similar Reynolds numbers, produced lower drag at $M = 0.35$ to 0.4 than at $M \approx 0.5$ to 0.6.

## Configuration D

Lift and drag characteristics obtained from the vehicle in configuration D at a flight Mach number of 0.6 and a Reynolds number of $25 \times 10^6$, based on the vehicle length, are presented in figures 16 and 17. Because configuration D is used at Mach numbers above 0.6, only limited results could be obtained during the glide-flight program; however, adequate data were available to define the lift and drag characteristics.

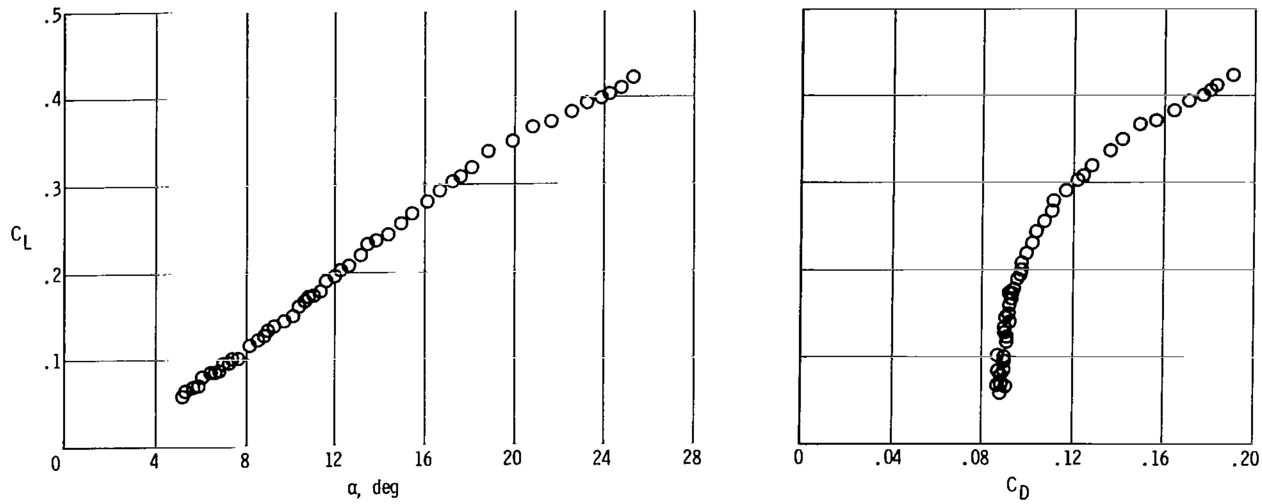


*(a) Lift curve and drag polar.*

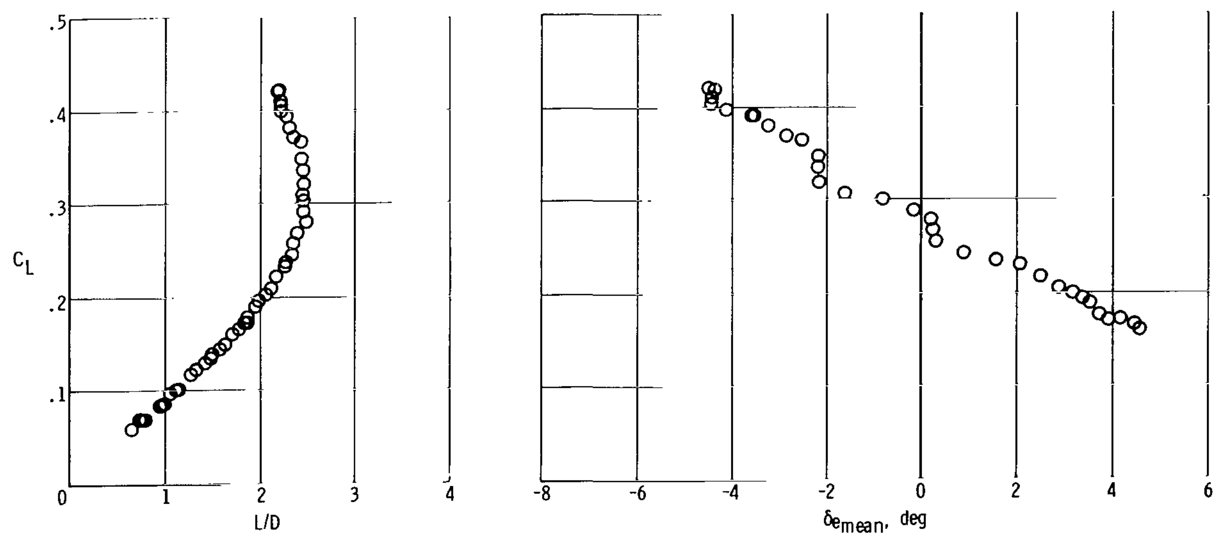


*(b) Lift-drag ratios and elevon deflections.*

*Figure 16. Lift and drag characteristics of the HL-10 vehicle in configuration D. M = 0.6.*

The effect of the speed brakes upon the lift and drag characteristics of configuration D and a comparison of the flight and small-scale wind-tunnel results are shown in figure 17. An increase of 8° in speed-brake deflection during flight tests produced an increase in drag coefficient of approximately 0.007 and a decrease of about 0.2 in lift-drag ratio for the vehicle in configuration D.

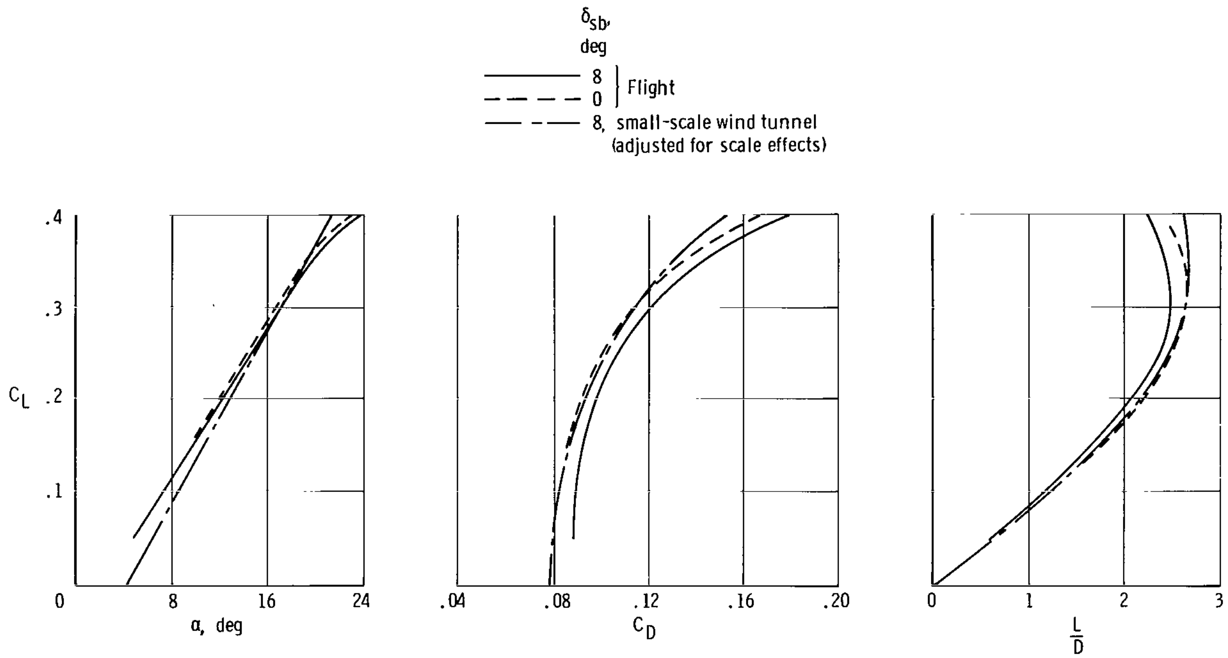


*Figure 17. Comparison of HL-10 flight results for configuration D with small-scale wind-tunnel results, and the effect of an 8° speed-brake deflection on the flight results. M = 0.6.*

The lift and drag parameters obtained from the flight tests and small-scale wind-tunnel tests for configuration D are presented in the following table:

| Test | $C_{L_\alpha}$ per deg | $(C_D)_{min}$ | $\frac{dC_D}{dC_L^2}$ | $\left(\frac{L}{D}\right)_{max}$ | $C_{L_{\delta_e}}$ per deg |
|---|---|---|---|---|---|
| Flight | 0.020 | 0.087 | 0.483 | 2.48 | 0.029 |
| Wind tunnel | .023 | .078 | .450 | 2.64 | .030 |

Comparison of the flight and wind-tunnel lift parameters shows close agreement; however, the drag results have some obvious differences. These differences are particularly noticeable in figure 17 which shows the displacement of the drag polars between flight and wind-tunnel data at common speed-brake settings.

## Effect of HL-10 Configuration Changes and Comparison of HL-10 and M2-F2 Flight Data

The flight-determined lift and drag parameters for three HL-10 configurations are compared in figure 18 and the table on page 23. These data are also compared with

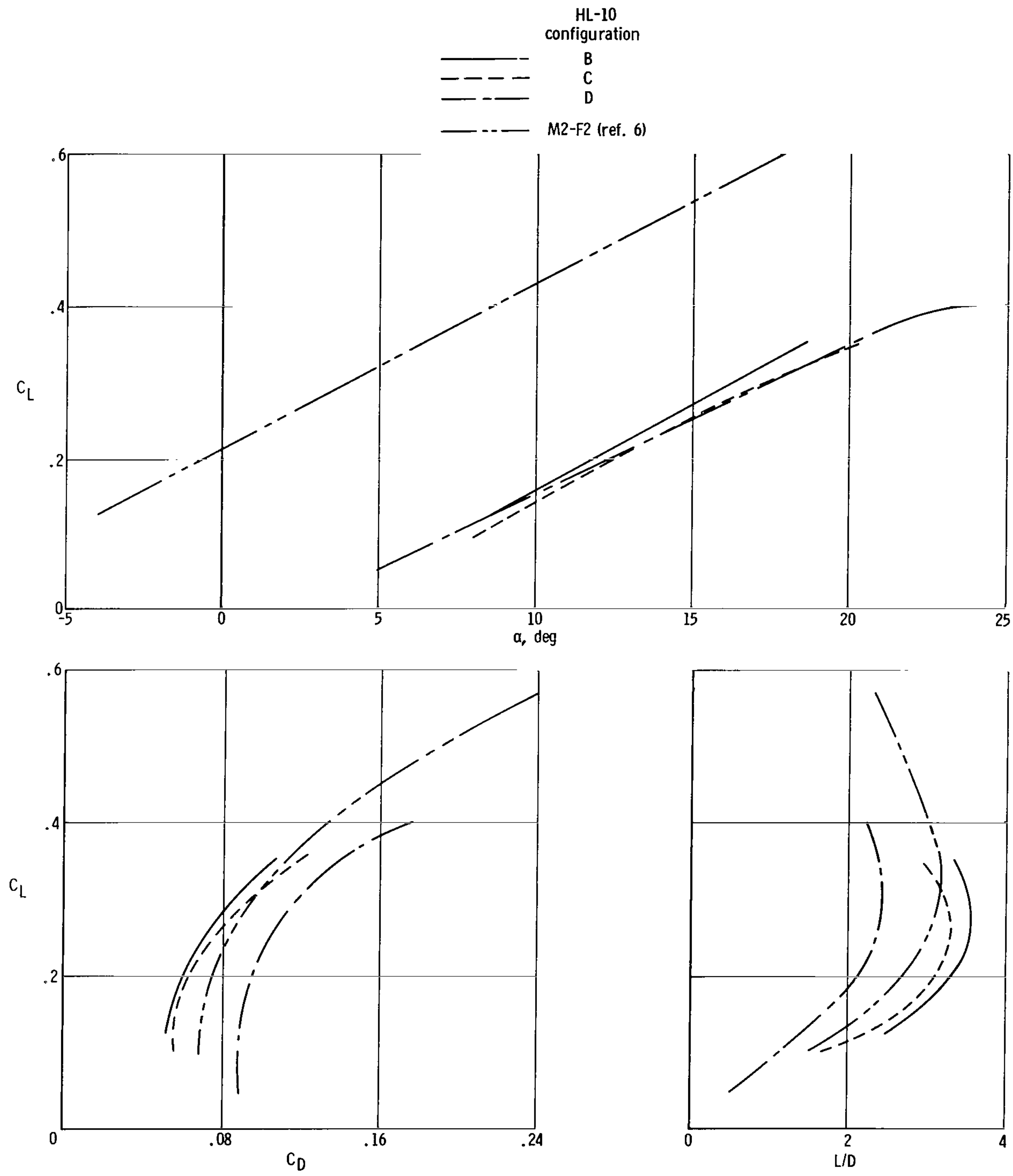


*Figure 18. Comparison of HL-10 flight results for configurations B, C, and D with flight results obtained from the M2-F2 lifting body vehicle. M = 0.6.*

| Vehicle | $C_{L_\alpha}$ per deg | $(C_D)_{min}$ | $\frac{dC_D}{dC_L^2}$ | $\left(\frac{L}{D}\right)_{max}$ |
|---|---|---|---|---|
| HL-10, Configuration B | 0.023 | 0.050 | 0.492 | 3.60 |
| HL-10, Configuration C | .021 | .055 | .571 | 3.33 |
| HL-10, Configuration D | .020 | .087 | .483 | 2.48 |
| M2-F2 | .022 | .063 | .505 | 3.16 |

corresponding data for the M2-F2 lifting body vehicle (ref. 6). The change in the secondary control deflections associated with modifying the HL-10 vehicle configuration from B to D increased the basic vehicle drag by as much as 74 percent. In modifying the vehicle configuration from B to C, the effect of the change in the secondary control deflections accounts for approximately 14 percent of the increase in $(C_D)_{min}$ associated with the modification from configurations B to D. Because the lift characteristics of all three configurations are similar, the lift-drag ratios are inversely proportional to the differences noted in the drag results.

Although the concept of a wingless vehicle was used in designing both the HL-10 and the M2-F2 lifting body vehicles, the configurations are quite dissimilar. A comparison of the lift and drag characteristics of each vehicle is presented in figure 18 and summarized in the above table. The similarity of the lift-curve slopes for both vehicles is of interest, even though the M2-F2 vehicle has a much lower angle of attack at a specific lift coefficient than the HL-10 vehicle. The maximum lift-drag ratio of the HL-10 vehicle in configuration B ($M = 0.6$) is 14 percent higher than the maximum lift-drag ratio measured with the M2-F2 vehicle.

The piloting tasks during the landing approach for the HL-10 and the M2-F2 vehicles are definitely different. The M2-F2 landing approach normally began at an angle of attack of approximately -2° (corresponding to a $C_L$ of about 0.15) along a glide slope of -25° (which is dependent upon the vehicle's lift-drag ratio). A typical landing approach for the HL-10 vehicle begins at an angle of attack of about 10° ($C_L$ slightly above 0.15) and a glide slope of -18°. Therefore, a typical HL-10 landing approach is performed at an attitude of -8°, whereas the M2-F2 attitude is approximately -27°. The pilots do not consider the steepness of the glide slopes to be detrimental to the overall landing task.

## CONCLUDING REMARKS

Subsonic lift and drag results were obtained from glide flights of the HL-10 lifting body vehicle in four configurations. These results indicated that the maximum lift-drag ratio (4.0) of the HL-10 vehicle was attained during the landing flare maneuver (performed with the landing gear up).

The lift and drag results obtained during the first HL-10 flight indicated a severe flow separation over the upper surface of the fuselage between Mach numbers of 0.5 and 0.6. The reduction of the basic drag of the vehicle after the tip fins were modified, when compared with the drag of the vehicle during the first flight, indicated a definite reduction of the flow separation over the vehicle's upper surface.

The maximum lift-drag ratio of the HL-10 vehicle was larger than that of the M2-F2 vehicle for similar configurations and Mach number ranges.

Flight Research Center,
National Aeronautics and Space Administration,
Edwards, Calif., November 20, 1970.

## REFERENCES


1. Ware, George M.: Aerodynamic Characteristics of Models of Two Thick 74° Delta Manned Lifting Entry Vehicles at Low-Subsonic Speeds. NASA TM X-914, 1964.

2. Rainey, Robert W.; and Ladson, Charles L.: Aerodynamic Characteristics of a Manned Lifting Entry Vehicle at Mach Numbers From 0.2 to 1.2. NASA TM X-1015, 1964.

3. Ware, George M.: Full-Scale Wind-Tunnel Investigation of the Aerodynamic Characteristics of the HL-10 Manned Lifting Entry Vehicle. NASA TM X-1160, 1965.

4. Harris, Charles D.: Effect of Elevon Deflection and of Model Components on Aerodynamic Characteristics of a Manned Lifting Entry Vehicle at Mach Numbers of 0.20 to 1.20. NASA TM X-1226, 1966.

5. Spencer, Bernard, Jr.; and Fox, Charles H., Jr.: Subsonic Longitudinal Control Characteristics of Several Elevon Configurations for a Manned Lifting Entry Vehicle. NASA TM X-1227, 1966.

6. Pyle, Jon S.; and Swanson, Robert H.: Lift and Drag Characteristics of the M2-F2 Lifting Body During Subsonic Gliding Flight. NASA TM X-1431, 1967.

7. Mechtly, E. A.: The International System of Units - Physical Constants and Conversion Factors. NASA SP-7012, 1964.

8. Gamse, Berl; and Mort, Kenneth W.: Full-Scale Wind-Tunnel Investigation of the HL-10 Manned Lifting Body Flight Vehicle. NASA TM X-1476, 1967.

9. McKinney, Linwood W.; and Huffman, Jarrett K.: Subsonic Aerodynamic Characteristics of a Model of the HL-10 Flight Research Vehicle With Basic and Modified Tip Fins. NASA TMX-2119, 1971.

10. Peterson, John B., Jr.: A Comparison of Experimental and Theoretical Results for the Compressible Turbulent-Boundary-Layer Skin Friction with Zero Pressure Gradient. NASA TN D-1795, 1963.

11. Beeler, De E.; Bellman, Donald R.; and Saltzman, Edwin J.: Flight Techniques for Determining Airplane Drag at High Mach Numbers. NACA TN 3821, 1956.

12. Larson, Terry J.; and Webb, Lannie D.: Calibrations and Comparisons of Pressure-Type Airspeed-Altitude Systems of the X-15 Airplane From Subsonic to High Supersonic Speeds. NASA TN D-1724, 1963.

13. Yaggy, Paul F.: A Method for Predicting the Upwash Angles Induced at the Propeller Plane for a Combination of Bodies With an Upswept Wing. NACA TN 2528, 1951.

14. Saltzman, Edwin J.; and Garringer, Darwin J.: Summary of Full-Scale Lift and Drag Characteristics of the X-15 Airplane. NASA TN D-3343, 1966.


NASA-Langley, 1971 —— 1 H-608

NATIONAL AERONAUTICS AND SPACE ADMINISTRATION
WASHINGTON, D.C. 20546

OFFICIAL BUSINESS

**FIRST CLASS MAIL**

POSTAGE AND FEES PAID
NATIONAL AERONAUTICS AND
SPACE ADMINISTRATION

05U 001 26 51 3DS 71058 00903
AIR FORCE WEAPONS LABORATORY /WLOL/
KIRTLAND AFB, NEW MEXICO 87117

ATT E. LOU BOWMAN, CHIEF,TECH. LIBRARY

POSTMASTER: If Undeliverable (Section 158 Postal Manual) Do Not Return

*"The aeronautical and space activities of the United States shall be conducted so as to contribute . . . to the expansion of human knowledge of phenomena in the atmosphere and space. The Administration shall provide for the widest practicable and appropriate dissemination of information concerning its activities and the results thereof."*

—NATIONAL AERONAUTICS AND SPACE ACT OF 1958

# NASA SCIENTIFIC AND TECHNICAL PUBLICATIONS

TECHNICAL REPORTS: Scientific and technical information considered important, complete, and a lasting contribution to existing knowledge.

TECHNICAL NOTES: Information less broad in scope but nevertheless of importance as a contribution to existing knowledge.

TECHNICAL MEMORANDUMS: Information receiving limited distribution because of preliminary data, security classification, or other reasons.

CONTRACTOR REPORTS: Scientific and technical information generated under a NASA contract or grant and considered an important contribution to existing knowledge.

TECHNICAL TRANSLATIONS: Information published in a foreign language considered to merit NASA distribution in English.

SPECIAL PUBLICATIONS: Information derived from or of value to NASA activities. Publications include conference proceedings, monographs, data compilations, handbooks, sourcebooks, and special bibliographies.

TECHNOLOGY UTILIZATION PUBLICATIONS: Information on technology used by NASA that may be of particular interest in commercial and other non-aerospace applications. Publications include Tech Briefs, Technology Utilization Reports and Technology Surveys.

*Details on the availability of these publications may be obtained from:*

**SCIENTIFIC AND TECHNICAL INFORMATION OFFICE**

**NATIONAL AERONAUTICS AND SPACE ADMINISTRATION**

**Washington, D.C. 20546**